Available online at www.sciencedirect.com
SCIENCE DIRECT
Journal of Sound and Vibration 295 (2006) 906–922
JOURNAL OF SOUND AND VIBRATION
www.elsevier.com/locate/jsvi

The element-free *kp*-Ritz method for free vibration analysis of conical shell panels

X. Zhao[a], Q. Li[b], K.M. Liew[c,*], T.Y. Ng[a]

[a]*Nanyang Centre for Supercomputing and Visualisation, Nanyang Technological University, 50 Nanyang Avenue, Singapore 639798, Singapore*
[b]*Shanghai Institute of Mathematics and Mechanics, Shanghai University, Shanghai 20072, P.R. China*
[c]*Department of Building and Construction, City University of Hong Kong, Kowloon, Hong Kong*

Received 14 January 2004; received in revised form 5 January 2006; accepted 27 January 2006
Available online 11 April 2006

Abstract

In this paper, the free vibration of conical panels is analyzed by the mesh-free *kp*-Ritz method. Both 1-D and 2-D versions of the *kp*-Ritz approach are formulated for conical panels. For conical panels with two simply supported straight edges, the 1-D *kp*-Ritz version is used, where the kernel particle estimation is employed in hybridized form with harmonic functions to approximate the 2-D displacement field. For conical panels having arbitrary boundary conditions, the displacement field is approximated by the 2-D *kp*-Ritz version, with 2-D form of kernel particle functions employed. The classical thin shell theory based on Love's hypothesis is employed in the present analyses, and based on the kernel particle concept and Ritz technique, the eigenequations of the frequencies of the conical panels are obtained. To validate the accuracy of stability of the present method, convergence studies were carried out based on the influences of the support size and the number of nodes. Comparisons were also made with existing results available in the open literature. This study also examines in detail the effects of variation in the semi-vertex angle and boundary conditions, on the frequency characteristics of conical panels.

1. Introduction

Conical shell panels are important structural components in engineering applications, such as in the aerospace and marine engineering disciplines. Therefore, the frequency characteristics of conical shell panels must be studied for safety and stability reasons. A very early work, Rossettos and Parisse [1], studied the dynamic responses of cylindrical and conical panels. Teichmann [2] provided an approximation of the lowest eigenfrequencies and buckling loads of cylindrical and conical shell panels under initial stresses. Srinivasan and Krishnan [3] solved the natural frequencies and modes of clamped isotropic conical panels using Donnell's shell theory and an integral equation technique. A spline finite strip method was developed by Cheung et al. [4] to study the free vibration of a singly curved shell panel. Lim and Liew [5] developed a global Ritz formulation based on the energy principle to study the free vibration of shallow conical shell panels. A set of orthogonally

*Corresponding author. Tel.: +852 3442 6581; fax: +852 2778 7612.
E-mail address: kmliew@cityu.edu.hk (K.M. Liew).

0022-460X/$ - see front matter © 2006 Elsevier Ltd. All rights reserved.
doi:10.1016/j.jsv.2006.01.045

generated and kinematically oriented *pb*-2 shape functions were used to approximate the displacement field. Based on the same method, the effects of initial twist and thickness variation on the vibration behaviour of shallow conical shells were investigated by Liew et al. [6]. Lim and Liew [7] also examined the vibration of shallow conical shells with shear flexibility. The derivation of thickness shear is assumed as a linear approximation, and the Lamé parameter for the transverse shear strain component was considered. Bardell et al. [8] performed the vibration analysis of thin, isotropic conical panels using the *h–p* finite element method in conjunction with Love's thin shell hypothesis. More recently, Liew and Feng [9] investigated the vibration characteristics of conical shell panels with 3-D flexibility, and Lam et al. [10] discussed the effects of boundary conditions on the free vibration characteristics of truncated conical panels using the generalized differential quadrature method.

The Ritz method is a numerical approach widely adopted in computational mechanics due to its simplicity, stability and efficiency in numerical implementation. It is a generalization of the Rayleigh [11] method, which is based on the principle that a resonant vibrating system completely interchanges its energy from a potential state to a kinetic state. In the Rayleigh method, a single trial function for the mode shape satisfying at least the geometric boundary conditions is employed, and then by equating the maximum kinetic and potential energies, an upper bound frequency solution is obtained accordingly. Ritz [12] extended Rayleigh method by using a set of admissible trial functions, each of which possesses an independent amplitude coefficient. From this, a more accurate upper bound solution may be obtained via minimizing the energy functional with respect to each of these coefficients. The Ritz approach was first successfully demonstrated by Ritz [12] for the analysis of a free square plate for which no exact solution exists.

In the Ritz method, the accuracy and convergence rate are highly dependent on the trial functions selected. The frequently used trial functions include the products of eigenfunctions of vibrating beams, 2-D orthogonal polynomials, and spline functions. Notable works include those of Liew and Lam [13–17], Liew [18–23], Liew and Wang [24], Liew and Lim [25], Liew and Sum [26], Liew and Yang [27], Liew and Feng [28], Liew et al. [29–32], Lim and Liew [33], Kitipornchai et al. [34], Cheung and Zhou [35–37]. In this paper, the vibration of conical panels with two simply supported straight edges is carried out based on the formulation of the 1-D version of the *kp*-Ritz method. This is then extended to the 2-D version of the *kp*-Ritz method for the vibration analysis of conical panels having arbitrary boundary conditions. Convergence studies based on the support size and number of nodes are performed to validate the accuracy as well as the stability of the present technique. Comparisons of the present results are also made with existing results available in open literature. Finally, the effects of boundary conditions and semi-vertex angle on the frequency characteristics of conical panels are elucidated.

2. Theoretical formulation—*kp*-Ritz method

2.1. Energy formulation

We begin with an energy analysis. A thin circular conical shell panel, as shown in Fig. 1, is considered, where the semi-vertex cone angle is denoted by α, the subtended angle by θ_o, the length by L, and the thickness by h. R_1 and R_2 are the radii at the two ends. A coordinate system (x, θ, z) is fixed on the mid-surface of the panel. The displacements of the shell panel in the x, θ and z directions are denoted by u, v, and w, respectively. The cone radius at any point along its length is given by

$$R(x) = R_1 + x \sin \alpha. \tag{1}$$

The kinetic energy for the circular conical shell panel can be expressed as

$$T = \frac{1}{2}\rho h \int_0^L \int_0^{\theta_o} [\dot{u}^2 + \dot{v}^2 + \dot{w}^2] R(x)\, \mathrm{d}\theta\, \mathrm{d}x, \tag{2}$$

where the three terms are due to contributions from the linear velocities in the x, θ and z directions, respectively.

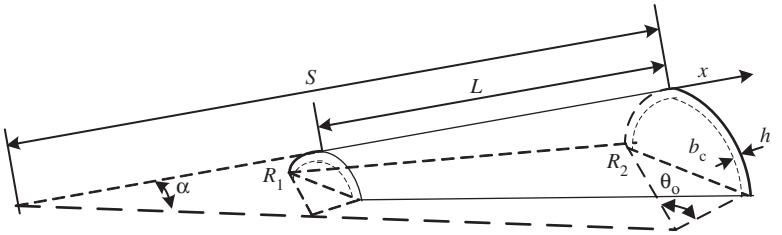

Fig. 1. Geometry of the circular conical shell panel.

The strain energy of the panel is given by

$$U_\varepsilon = \frac{1}{2}\int_0^L \int_0^{\theta_o} \boldsymbol{\varepsilon}^{\mathrm{T}} \mathbf{S} \boldsymbol{\varepsilon} R(x)\,\mathrm{d}\theta\,\mathrm{d}x, \tag{3}$$

where $\boldsymbol{\varepsilon}^{\mathrm{T}}$ and $\mathbf{S}$ are the strain vector and stiffness matrix, respectively, and $\boldsymbol{\varepsilon}^{\mathrm{T}}$ is defined as

$$\boldsymbol{\varepsilon}^{\mathrm{T}} = \{e_1 \quad e_2 \quad \gamma \quad \kappa_1 \quad \kappa_2 \quad 2\tau\}, \tag{4}$$

where the middle surface strains e_1, e_2 and γ and the middle surface curvatures κ_1, κ_2 and τ are defined according to Love's thin shell theory as follows

$$e_1 = \frac{\partial u}{\partial x}, \quad e_2 = \frac{1}{R(x)}\frac{\partial v}{\partial \theta} + \frac{u\sin\alpha}{R(x)} + \frac{w\cos\alpha}{R(x)}, \quad \gamma = \frac{\partial v}{\partial x} + \frac{1}{R(x)}\frac{\partial u}{\partial \theta} - \frac{v\sin\alpha}{R(x)}, \tag{5}$$

$$\kappa_1 = -\frac{\partial^2 w}{\partial^2 x}, \quad \kappa_2 = -\frac{1}{R^2(x)}\frac{\partial^2 w}{\partial^2 \theta} + \frac{\cos\alpha}{R^2(x)}\frac{\partial v}{\partial \theta} - \frac{\sin\alpha}{R(x)}\frac{\partial w}{\partial x}, \tag{6}$$

$$\tau = -\frac{1}{R(x)}\frac{\partial^2 w}{\partial x \partial \theta} + \frac{\cos\alpha}{R(x)}\frac{\partial v}{\partial x} + \frac{\sin\alpha}{R^2(x)}\frac{\partial w}{\partial \theta} - \frac{v\sin\alpha\cos\alpha}{R^2(x)}. \tag{7}$$

The stiffness matrix $\mathbf{S}$ is given by

$$\mathbf{S} = \begin{bmatrix} A_{11} & A_{12} & A_{16} & B_{11} & B_{12} & B_{16} \\ A_{12} & A_{22} & A_{26} & B_{12} & B_{22} & B_{26} \\ A_{16} & A_{26} & A_{66} & B_{16} & B_{26} & B_{66} \\ B_{11} & B_{12} & B_{16} & D_{11} & D_{12} & D_{16} \\ B_{12} & B_{22} & B_{26} & D_{12} & D_{22} & D_{26} \\ B_{16} & B_{26} & B_{66} & D_{16} & D_{26} & D_{66} \end{bmatrix}, \tag{8}$$

where the extensional stiffnesses A_{ij}, and bending stiffnesses D_{ij} are defined as

$$(A_{ij}, D_{ij}) = \int_{-h/2}^{h/2} Q_{ij}(1, z^2)\,\mathrm{d}z \tag{9}$$

and Q denotes the plane stress-reduced stiffness matrix

$$Q = \begin{bmatrix} Q_{11} & Q_{12} & 0 \\ Q_{12} & Q_{22} & 0 \\ 0 & 0 & Q_{66} \end{bmatrix} \tag{10}$$

with

$$Q_{11} = \frac{E}{1-\vec{v}^2}, \quad Q_{12} = \frac{vE}{1-\vec{v}^2}, \quad Q_{22} = \frac{E}{1-\vec{v}^2}, \quad Q_{66} = G, \tag{11}$$

where E is the elastic modulus, G the shear modulus, and $\bar{v}$ the Poisson's ratio. Thus, the energy functional of the conical shell panel can be written as

$$\Gamma_t = T - U_\varepsilon. \tag{12}$$

2.2. 1-D kernel particle (kp) shape functions

For the conical panel having simply supported straight edges, the boundary conditions at these two straight edges are expressed as

$$u = w = 0 \quad \text{at } \theta = 0, \theta_o. \tag{13}$$

For such a conical shell panel, an admissible set of displacement functions are expressed as follows

$$u(x,\theta) = \sum_{I=1}^{NP} \psi_I(x) u_I \sin\frac{n\pi\theta}{\theta_o}\cos\omega t, \tag{14a}$$

$$v(x,\theta) = \sum_{I=1}^{NP} \psi_I(x) v_I \cos\frac{n\pi\theta}{\theta_o}\cos\omega t, \tag{14b}$$

$$w(x,\theta) = \sum_{I=1}^{NP} \psi_I(x) w_I \sin\frac{n\pi\theta}{\theta_o}\cos\omega t, \tag{14c}$$

where NP is the total number of particles, and $\psi_I(x)$ is the axial shape function. u_I, v_I and w_I are the unknown nodal values of u, v and w at a given point, and n is the circumferential half wavenumber.

The shape function is given by, see Chen et al. [38] and Liu et al. [39],

$$\psi_I(x) = C(x; x - x_I)\phi_a(x - x_I), \tag{15}$$

where $C(x; x - x_I)$ is the correction function and $\phi_a(x - x_I)$ is called the kernel function.

The correction function $C(x; x - x_I)$ is written as

$$C(x; x - x_I) = \mathbf{H}^{\mathrm{T}}(x - x_I)\mathbf{b}(x), \tag{16}$$

where

$$\mathbf{H}(x - x_I) = [1, x - x_I, (x - x_I)^2]^{\mathrm{T}} \tag{17}$$

$$\mathbf{b}(x) = [b_0(x), b_1(x), b_2(x)]^{\mathrm{T}} \tag{18}$$

in which $\mathbf{H}$ is a vector of quadratic basis, and $b_i(x)$ are functions of x which are to be determined.

Thus, the shape functions can be assembled as

$$\psi_I(x) = \mathbf{b}^{\mathrm{T}}(x)\mathbf{H}(x - x_I)\phi_a(x - x_I) \tag{19}$$

and Eq. (19) can be rewritten as

$$\psi_I(x) = \mathbf{b}^{\mathrm{T}}(x)\mathbf{B}_I(x - x_I) \tag{20}$$

in which

$$\mathbf{B}_I(x - x_I) = \mathbf{H}(x - x_I)\phi_a(x - x_I) \tag{21}$$

$$\mathbf{b}(x) = \boldsymbol{\eta}^{-1}(x)\mathbf{H}(0), \tag{22}$$

where the entries of moment matrix $\boldsymbol{\eta}$ are functions of x, and $\mathbf{H}(0)$ is a constant vector.

The expressions of $\boldsymbol{\eta}$ and $\mathbf{H}(0)$ are given by

$$\boldsymbol{\eta}(x) = \sum_{I=1}^{NP} \mathbf{H}(x - x_I)\mathbf{H}^{\mathrm{T}}(x - x_I)\phi_a(x - x_I), \tag{23}$$

$$\mathbf{H}^{\mathrm{T}}(0) = [1, 0, 0]. \tag{24}$$

Therefore, the shape function can be expressed as

$$\psi_I(x) = \mathbf{H}^{\mathrm{T}}(0)\boldsymbol{\eta}^{-1}(x)\mathbf{H}(x - x_I)\phi_a(x - x_I). \tag{25}$$

For thin shell problems, due to the governing differential equations being second order, the first and second derivatives of the shape functions need to be determined.

The first derivative of the shape function can be obtained by taking the derivative of Eq. (25), i.e.

$$\psi_{I,x}(x) = \mathbf{b}_{,x}^{\mathrm{T}}(x)\mathbf{B}_I(x - x_I) + \mathbf{b}^{\mathrm{T}}(x)\mathbf{B}_{I,x}(x - x_I). \tag{26}$$

The second derivative of the shape function can be determined by taking derivative of Eq. (26) again, i.e.

$$\psi_{I,xx}(x) = \mathbf{b}_{,xx}^{\mathrm{T}}(x)\mathbf{B}_I(x - x_I) + 2\mathbf{b}_{,x}^{\mathrm{T}}(x)\mathbf{B}_{I,x}(x - x_I) + \mathbf{b}^{\mathrm{T}}(x)\mathbf{B}_{I,xx}(x - x_I). \tag{27}$$

The kernel function is expressed as, see Chen et al. [38] and Liu et al. [39],

$$\phi_a = \frac{1}{d}\phi\left(\frac{x - x_I}{d}\right), \tag{28}$$

where the dilation parameter d is the size of the support and $\phi((x - x_I)/d)$ is the weight function. In this study, cubic spline functions are chosen as the weights

$$\phi(z_I) = \begin{cases} \frac{2}{3} - 4z_I^2 + 4z_I^3 & \text{for} \quad 0 \leqslant |z_I| \leqslant \frac{1}{2}, \\ \frac{4}{3} - 4z_I + 4z_I^2 - \frac{4}{3}z_I^3 & \text{for} \quad \frac{1}{2} \leqslant |z_I| \leqslant 1, \\ 0 & \text{otherwise}, \end{cases} \tag{29a}$$

$$z_1 = \frac{(x - x_I)}{d}. \tag{29b}$$

At a node, the size of the domain of influence is calculated by

$$d_I = d_{\max} a_I, \tag{30}$$

where $d_{\max}$ is the scaling factor, which generally ranges from 2.0 to 4.0. The distance a_I is determined by searching for sufficient nodes so as to avoid singularity of the matrix $\boldsymbol{\eta}$. For a 1-D problem, each node should have at least two neighboring nodes in its domain of influence.

2.3. 2-D kernel particle (kp) shape functions

For conical panels with arbitrary boundary conditions, the discrete displacement approximations take the form

$$u(x, \theta) = \sum_{I=1}^{NP} \Psi_I(x, \theta) u_I e^{i\omega t}, \tag{31a}$$

$$v(x, \theta) = \sum_{I=1}^{NP} \Psi_I(x, \theta) v_I e^{i\omega t}, \tag{31b}$$

$$w(x, \theta) = \sum_{I=1}^{NP} \Psi_I(x, \theta) w_I e^{i\omega t}, \tag{31c}$$

where the 2-D shape function $\Psi_I(x, \theta)$ is constructed in similar fashion to the procedure described above for the corresponding 1-D case. However, the unknown coefficients and quadratic base vector in Eq. (21) are now given as

$$\mathbf{b}(\mathbf{x}) = [b_0(x, \theta), b_1(x, \theta), b_2(x, \theta), b_3(x, \theta), b_4(x, \theta), b_5(x, \theta)]^{\mathrm{T}}, \tag{32}$$

$$\mathbf{H}(\mathbf{x}-\mathbf{x}_I)=[1,x-x_I,\theta-\theta_I,(x-x_I)(\theta-\theta_I),(x-x_I)^2,(\theta-\theta_I)^2]^{\mathrm{T}}. \tag{33}$$

For this 2-D problem, the weight function is expressed as, see Chen et al. [38]

$$\Psi(x,\theta)=\phi(x)\phi(\theta), \tag{34}$$

where the weight functions $\phi(x)$ and $\phi(\theta)$ are of the same forms as in Eq. (29).

2.4. Penalty enforcement of essential boundary conditions

In the present work, we consider different boundary conditions. The penalty method, see Reddy [40,41], is utilized to implement the essential boundary conditions. The penalty formulation is described as follows:

2.4.1. Simply supported boundary conditions

For the domain bounded by l_u, the displacement boundary condition is

$$\mathbf{u}=\bar{\mathbf{u}} \tag{35}$$

in which $\bar{\mathbf{u}}$ is the prescribed displacement on the displacement boundary l_u. Eq. (35) is treated as a constraint condition and it is introduced into the formulation using the penalty method. The variational form of the penalty functional is given by

$$\Gamma_{\bar{u}}=\frac{\bar{\alpha}}{2}\int_{l_u}(\mathbf{u}-\bar{\mathbf{u}})^{\mathrm{T}}(\mathbf{u}-\bar{\mathbf{u}})\,\mathrm{d}l, \tag{36}$$

where $\bar{\alpha}$ is the penalty parameter, which is taken to be 10^3E, with E being the elastic modulus of the shell.

2.4.2. Clamped boundary conditions

For the clamped case, in the domain bounded by l_u, besides the boundary condition described by Eq. (35), the restriction to rotation must also be included

$$\boldsymbol{\beta}=\bar{\boldsymbol{\beta}}, \tag{37}$$

where

$$\boldsymbol{\beta}=\frac{\mathrm{d}w}{\mathrm{d}x} \tag{38}$$

and $\bar{\boldsymbol{\beta}}$ is the prescribed rotation on the boundary.

The variational form due to the rotational constraint of Eq. (37) is given by

$$\Gamma_{\bar{\beta}}=\frac{\bar{\alpha}}{2}\int_{l_u}(\boldsymbol{\beta}-\bar{\boldsymbol{\beta}})^{\mathrm{T}}(\boldsymbol{\beta}-\bar{\boldsymbol{\beta}})\,\mathrm{d}l. \tag{39}$$

Although in general the penalty parameter for each constraint can be taken differently, here the same penalty parameter is used for both boundary constraint types.

2.5. Ritz minimization

The variational form due to the boundary conditions can be expressed as

$$\Gamma_B=\Gamma_{\bar{u}}+\Gamma_{\bar{\beta}} \tag{40}$$

and the total energy functional for the conical panel thus becomes

$$\Gamma=\Gamma_t+\Gamma_B. \tag{41}$$

Applying the Ritz minimization procedure to the energy functional

$$\frac{\partial\Gamma}{\partial u_I}=\frac{\partial\Gamma}{\partial v_I}=\frac{\partial\Gamma}{\partial w_I}=0,\quad I=1,2,\ldots,NP \tag{42}$$

the matrix equation of the conical shell panel can be obtained as

$$(\tilde{\mathbf{K}} - \omega^2 \tilde{\mathbf{M}})\hat{\mathbf{u}} = 0, \tag{43}$$

where

$$\tilde{\mathbf{K}} = \mathbf{\Lambda}^{-1}\mathbf{K}\mathbf{\Lambda}^{-\mathrm{T}}, \quad \tilde{\mathbf{M}} = \mathbf{\Lambda}^{-1}\mathbf{M}\mathbf{\Lambda}^{-\mathrm{T}}, \tag{44}$$

$$\mathbf{K} = \mathbf{K}^{\varepsilon} + \mathbf{K}^{B_1} + \mathbf{K}^{B_2}. \tag{45}$$

Taking Eq. (14) as the displacement functions in the 1-D *kp*-Ritz approximation, the system matrices are given as follows

$$\mathbf{\Lambda}_{IJ} = \psi_I(x_J)\mathbf{I}, \quad \mathbf{I} \text{ is an identity matrix}, \tag{46}$$

$$\mathbf{K}_{IJ}^{B_1} = \frac{\bar{\alpha}\theta_o}{2}\left(\int_{l_u} \mathbf{B}1_I^{B^{\mathrm{T}}}\mathbf{B}1_J^B R(x)\,\mathrm{d}l + \int_{l_u} \mathbf{B}1_I^B \bar{\mathbf{u}} R(x)\,\mathrm{d}l\right), \tag{47}$$

$$\mathbf{K}_{IJ}^{B_2} = \frac{\bar{\alpha}\theta_o}{2}\left(\int_{l_u} \mathbf{B}2_I^{B^{\mathrm{T}}}\mathbf{B}2_J^B R(x)\,\mathrm{d}l + \int_{l_u} \mathbf{B}2_I^B \bar{\boldsymbol{\beta}} R(x)\,\mathrm{d}l\right), \tag{48}$$

$$\mathbf{K}_{IJ}^{\varepsilon} = \frac{\theta_o}{2}\int_0^L \mathbf{B}_I^{\varepsilon\mathrm{T}}\mathbf{S}\mathbf{B}_J^{\varepsilon} R(x)\,\mathrm{d}x, \quad \mathbf{M} = \frac{\rho h\theta_o}{2}\int_0^L \mathbf{M}_I^{\mathrm{T}}\mathbf{M}_J R(x)\,\mathrm{d}x, \tag{49}$$

$$\mathbf{B}_I^{\varepsilon} = \begin{bmatrix} \dfrac{\partial\psi_I}{\partial x} & 0 & 0 \\ \dfrac{\sin\alpha}{R(x)}\psi_I & \dfrac{n\pi}{\theta_o R(x)}\psi_I & \dfrac{\cos\alpha}{R(x)}\psi_I \\ -\dfrac{n\pi}{\theta_o R(x)}\psi_I & \dfrac{\partial\psi_I}{\partial x} - \dfrac{\sin\alpha}{R(x)}\psi_I & 0 \\ 0 & 0 & -\dfrac{\partial^2\psi_I}{\partial x^2} \\ 0 & \dfrac{n\pi\cos\alpha}{\theta_o R^2(x)}\psi_I & \dfrac{n^2\pi}{\theta_o R^2(x)}\psi_I - \dfrac{\sin\alpha}{R(x)}\dfrac{\partial\psi_I}{\partial x} \\ 0 & \dfrac{2\cos\alpha}{R(x)}\dfrac{\partial\psi_I}{\partial x} - \dfrac{2\sin\alpha\cos\alpha}{R^2(x)}\psi_I & \dfrac{2n\pi}{\theta_o R(x)}\dfrac{\partial\psi_I}{\partial x} - \dfrac{2n\pi\sin\alpha}{\theta_o R^2(x)}\psi_I \end{bmatrix}, \tag{50}$$

$$\mathbf{B}1_I^B = \begin{bmatrix} \psi_I & 0 & 0 \\ 0 & \psi_I & 0 \\ 0 & 0 & \psi_I \end{bmatrix}, \quad \mathbf{B}2_I^B = \begin{bmatrix} \psi_{I,x} & 0 & 0 \\ 0 & \psi_{I,x} & 0 \\ 0 & 0 & \psi_{I,x} \end{bmatrix}, \tag{51}$$

$$\mathbf{M}_I^{\mathrm{T}} = \begin{bmatrix} \psi_I & 0 & 0 \\ 0 & \psi_I & 0 \\ 0 & 0 & \psi_I \end{bmatrix}. \tag{52}$$

Taking Eq. (31) as the displacement functions in the 2-D *kp*-Ritz approximation, the system matrices are given as follows:

$$\mathbf{\Lambda}_{IJ} = \Psi_I(x_J)\mathbf{I}, \quad \mathbf{I} \text{ is an identity matrix}, \tag{53}$$

$$\mathbf{K}_{IJ}^{\varepsilon} = \int_0^L \int_0^{\theta_o} \mathbf{B}_I^{\varepsilon\mathrm{T}}\mathbf{S}\mathbf{B}_J^{\varepsilon} R(x)\,\mathrm{d}\theta\,\mathrm{d}x, \tag{54}$$

$$\mathbf{K}_{IJ}^{B_1} = \bar{\alpha}\left(\int_{l_u} \mathbf{B}1_I^{B^{\mathrm{T}}} \mathbf{B}1_J^B R(x)\,\mathrm{d}l + \int_{l_u} \mathbf{B}1_I^B \bar{\mathbf{u}} R(x)\,\mathrm{d}l\right), \tag{55}$$

$$\mathbf{K}_{IJ}^{B_2} = \bar{\alpha}\left(\int_{l_u} \mathbf{B}2_I^{B^{\mathrm{T}}} \mathbf{B}2_J^B R(x)\,\mathrm{d}l + \int_{l_u} \mathbf{B}2_I^B \bar{\boldsymbol{\beta}} R(x)\,\mathrm{d}l\right), \tag{56}$$

$$\mathbf{M}_{IJ} = \rho h \int_0^L \int_0^{\theta_o} \mathbf{M}_I^{\mathrm{T}} \mathbf{M}_J R(x)\,\mathrm{d}\theta\,\mathrm{d}x, \tag{57}$$

$$\mathbf{B}_I^{\varepsilon} = \begin{bmatrix} \dfrac{\partial \Psi_I}{\partial x} & 0 & 0 \\ \dfrac{\sin\alpha}{R(x)}\Psi_I & \dfrac{1}{R(x)}\dfrac{\partial \Psi_I}{\partial \theta} & \dfrac{\cos\alpha}{R(x)}\Psi_I \\ \dfrac{1}{R(x)}\dfrac{\partial \Psi_I}{\partial \theta} & \dfrac{\partial \Psi_I}{\partial x} - \dfrac{\sin\alpha}{R(x)}\Psi_I & 0 \\ 0 & 0 & -\dfrac{\partial^2 \Psi_I}{\partial x^2} \\ 0 & \dfrac{\cos\alpha}{R^2(x)}\dfrac{\partial \Psi_I}{\partial \theta} & -\dfrac{1}{R^2(x)}\dfrac{\partial^2 \Psi_I}{\partial \theta^2} - \dfrac{\sin\alpha}{R(x)}\dfrac{\partial \Psi_I}{\partial x} \\ 0 & \dfrac{2\cos\alpha}{R(x)}\dfrac{\partial \Psi_I}{\partial x} - \dfrac{2\cos\alpha\sin\alpha}{R^2(x)}\Psi_I & -\dfrac{2}{R(x)}\dfrac{\partial^2 \Psi_I}{\partial x \partial \theta} + \dfrac{2\sin\alpha}{R^2(x)}\dfrac{\partial \Psi_I}{\partial \theta} \end{bmatrix}, \tag{58}$$

$$\mathbf{B}1_I^B = \begin{bmatrix} \Psi_I & 0 & 0 \\ 0 & \Psi_I & 0 \\ 0 & 0 & \Psi_I \end{bmatrix}, \quad \mathbf{B}2_I^B = \begin{bmatrix} \Psi_{I,x} & 0 & 0 \\ 0 & \Psi_{I,x} & 0 \\ 0 & 0 & \Psi_{I,x} \end{bmatrix}, \tag{59}$$

$$\mathbf{M} = \begin{bmatrix} \Psi_I & 0 & 0 \\ 0 & \Psi_I & 0 \\ 0 & 0 & \Psi_I \end{bmatrix}. \tag{60}$$

The above integrations can be carried out using Gauss integration, and the global mass and stiffness matrices can be obtained by assembling the elemental matrices with overlapping at common nodes, in similar fashion as finite elements.

3. Numerical results and discussions

3.1. Conical panels with simply supported straight edges

In this section, the frequency results for conical panels with simply supported straight edges are obtained using the 1-D *kp*-Ritz method. To evaluate the validity and the accuracy of the present formulation, convergence and comparison studies are performed. Table 1 shows the comparison of frequency parameter

$$\hat{f} = \omega R_2 \sqrt{\frac{\rho h}{A_{11}}} \tag{61}$$

for conical panels having S_S–S_L boundary condition, with results presented by Lam et al. [10]. S_S–S_L represents simply supported boundary conditions, where the subscripts "S" and "L" refer to the arcs at the small and large ends, respectively. The conical shell panel has geometrical parameters

Table 1
Comparison of frequency parameter $\hat{f} = \omega R_2\sqrt{\rho h/A_{11}}$ for conical panels with S_S–S_L boundary conditions ($m = 1, \alpha = 20^\circ, \theta_o = 60^\circ, \nu = 0.3, h/R_1 = 0.015, L/R_1 = 20$)

n	Lam et al. [10]		Present 1-D kp-Ritz											
	GDQ	Nastran	$d_{\max} = 2.0$				$d_{\max} = 2.5$				$d_{\max} = 3.0$			
			$NP = 20$	$NP = 40$	$NP = 60$	$NP = 80$	$NP = 20$	$NP = 40$	$NP = 60$	$NP = 80$	$NP = 20$	$NP = 40$	$NP = 60$	$NP = 80$
2	0.0638	0.0655	0.0656	0.0655	0.0655	0.0655	0.0655	0.0655	0.0655	0.0655	0.0655	0.0655	0.0655	0.0655
3	0.0909	0.0917	0.0919	0.0918	0.0918	0.0918	0.0918	0.0917	0.0917	0.0917	0.0918	0.0917	0.0917	0.0917
4	0.1299	0.1301	0.1310	0.1306	0.1306	0.1305	0.1309	0.1305	0.1304	0.1304	0.1312	0.1305	0.1305	0.1305
5	0.1801	0.1797	0.1820	0.1810	0.1809	0.1808	0.1820	0.1809	0.1808	0.1808	0.1826	0.1810	0.1808	0.1808
6	0.2419	0.2401	0.2450	0.2429	0.2426	0.2425	0.2452	0.2428	0.2425	0.2424	0.2463	0.2430	0.2425	0.2424
7	0.3147	0.3109	0.3198	0.3162	0.3157	0.3155	0.3200	0.3161	0.3155	0.3154	0.3217	0.3166	0.3157	0.3154

Table 2
Comparison of frequency parameter $\hat{f} = \omega R_2\sqrt{\rho h/A_{11}}$ for conical panels with C_S–C_L boundary conditions ($m = 1, n = 2, \theta_o = 60^\circ, \nu = 0.3, h/R_1 = 0.02, L/R_1 = 25$)

α	Lam et al. [10]		Present 1-D kp-Ritz											
	GDQ	Nastran	$d_{\max} = 2.0$				$d_{\max} = 2.5$				$d_{\max} = 3.0$			
			$NP = 20$	$NP = 40$	$NP = 60$	$NP = 80$	$NP = 20$	$NP = 40$	$NP = 60$	$NP = 80$	$NP = 20$	$NP = 40$	$NP = 60$	$NP = 80$
10	0.0850	0.0847	0.0856	0.0851	0.0849	0.0849	0.0852	0.0849	0.0848	0.0848	0.0849	0.0847	0.0847	0.0847
20	0.0937	0.0934	0.0942	0.0938	0.0936	0.0936	0.0939	0.0936	0.0935	0.0935	0.0936	0.0934	0.0934	0.0934
30	0.1104	0.1102	0.1112	0.1106	0.1104	0.1104	0.1107	0.1103	0.1102	0.1102	0.1104	0.1102	0.1102	0.1102
40	0.1240	0.1290	0.1251	0.1244	0.1242	0.1242	0.1246	0.1242	0.1241	0.1241	0.1243	0.1240	0.1240	0.1240

$\alpha = 20^\circ, \theta_o = 60^\circ, h/R_1 = 0.015$, and $L/R_1 = 20$. The support size varies from 2.0 to 3.0, and the number of nodes ranges from 20 to 80. It is observed that the present method possesses good convergence characteristics for all three support sizes considered. Also, good agreement with Lam et al. [10] is observed from the comparisons. Next, the influences of the semi-vertex angle α on the convergence rates are investigated. The convergence characteristics of C_S–C_L conical panels with various values of α are shown in Table 2. It is found that α have no significant additional effects on convergence rates. Again, good agreement with Lam et al. [10] is observed for these two cases.

The variation of the frequency parameter $\hat{f}$ with the semi-vertex angle α for a conical panel having S_S–S_L boundary conditions is given in Fig. 2. For a conical panel with $\theta_o = 30^\circ$, it is observed that the frequencies for mode $n = 1$ increase as α increases, while the frequencies decrease with increasing α, for modes $n = 2$ to 5. The same trends are observed for a corresponding conical panel with $\theta_o = 60^\circ$ for modes $n = 1$, 3, 4 and 5. However, the frequencies for mode $n = 2$, show a different trend. Fig. 3 shows the variation of frequency with α for a conical panel having C_S–C_L boundary conditions. For such a panel with $\theta_o = 30^\circ$ modes $n = 2$, 3, 4 and 5 show the same trends as the preceding simply supported case in Table 5, while for $n = 1$, the frequencies initially increase with α, up to $\alpha = 50^\circ$, and as α is increased further, the frequencies then decrease. For corresponding conical panels having S_S–C_L boundary conditions, see Fig. 4, the variation of frequencies with α, θ_o and n are very similar as those in Fig. 3 for corresponding modes of the C_S–C_L case. The same observations are also made in Figs. 5–7, for corresponding frequency results of conical panels with respective C_S–S_L, F_S–F_L (free curved edges) and F_S–C_L boundary conditions.

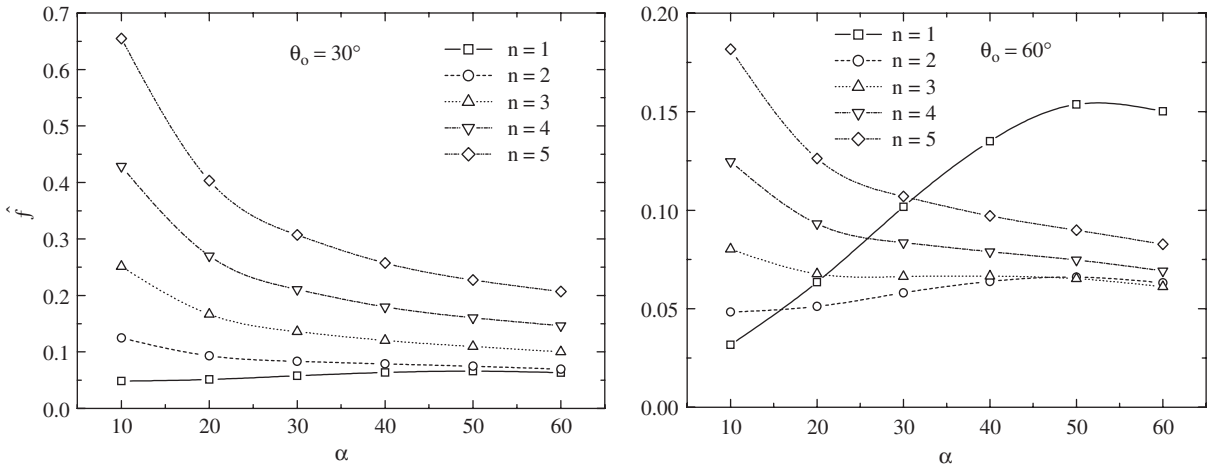

Fig. 2. Frequency parameter $\hat{f} = \omega b\sqrt{\rho h/A_{11}}$ of conical panels with S_S–S_L boundary conditions ($m = 1, v = 0.3, h/R_1 = 0.01, L/R_1 = 20$).

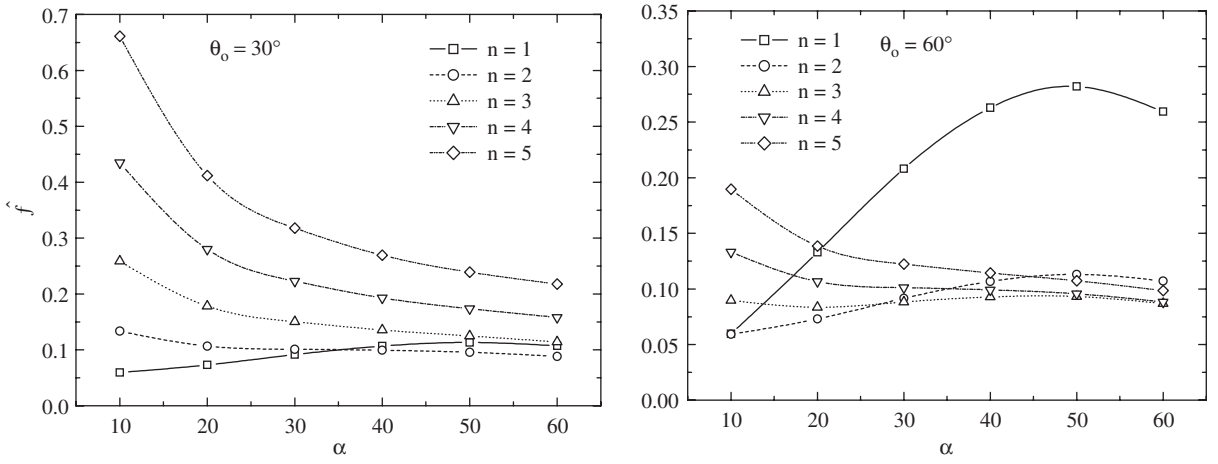

Fig. 3. Frequency parameter $\hat{f} = \omega b\sqrt{\rho h/A_{11}}$ of conical panels with C_S–C_L boundary conditions ($m = 1, v = 0.3, h/R_1 = 0.01, L/R_1 = 20$).

3.2. Conical panels with arbitrary boundary conditions

In this section, the results are obtained by using the 2-D *kp*-Ritz method. In order to verify the present formulation, comparisons with those available in open literature are made. The first comparison concerns the example given by Cheung et al. [4], who presented results of the dimensionless frequency parameter

$$\tilde{f} = \omega L^2\sqrt{\frac{\rho h}{D}} \tag{62}$$

for a fully clamped conical shell panel using the spline finite stripe method. This case was first analyzed by Srinivasan and Krishnan [3], and was later also studied by Bardell et al. [8] using the *h*–*p* version finite element method. This shell panel is defined by $L/s = 0.6$, $L/h = 100$, $L/R_1 = 3$, $\alpha = 30^\circ$, $\theta_o = 60^\circ$, and $v = 0.3$. The present converged results are obtained using a support size of 3.5. The comparisons are detailed in Table 3. It is observed that the fundamental frequency agrees well with the results of both Cheung et al. [4] and

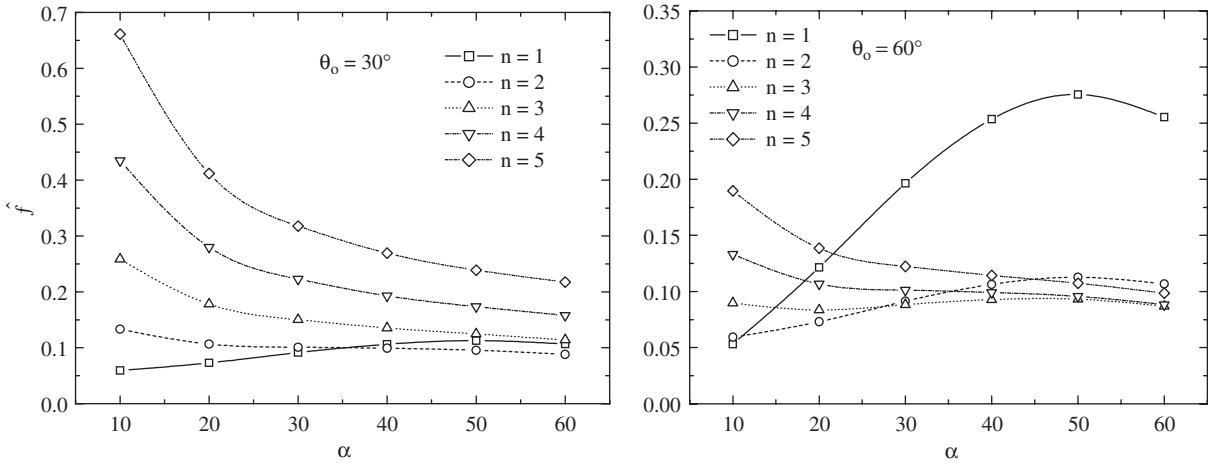

Fig. 4. Frequency parameter $\hat{f} = \omega b\sqrt{\rho h/A_{11}}$ of conical panels with S_S–C_L boundary conditions ($m = 1, v = 0.3, h/R_1 = 0.01, L/R_1 = 20$).

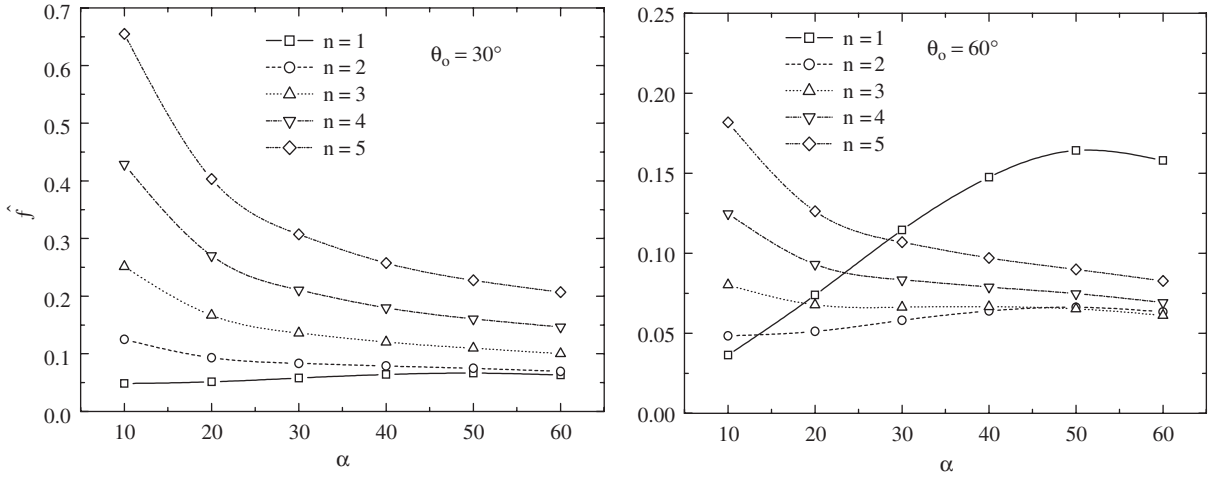

Fig. 5. Frequency parameter $\hat{f} = \omega b\sqrt{\rho h/A_{11}}$ of conical panels with C_S–S_L boundary conditions ($m = 1, v = 0.3, h/R_1 = 0.01, L/R_1 = 20$).

Bardell et al. [8]. The present solutions for the other three frequencies are little higher, but maximum differences do not exceed 5%.

Table 4 shows another comparison of present results for the frequency parameter

$$\bar{f} = \omega L b_o \sqrt{\frac{\rho h}{D}} \tag{63}$$

with those reported by Lim and Liew [5] and Bardell et al. [8], for conical panels having CFFF boundary conditions. The panels are clamped at the larger curved end. The panel parameters are $L/R_1 = 3$, $\alpha = 75^\circ$, $\theta_o = 30.247^\circ$, $v = 0.3$ and $L/s = 0.2$ and 0.8. The first eight modes of each case are presented. The present converged solutions are achieved using 22×22 nodes and support size of 3.5. It is observed that generally good agreement is attained with Bardell et al. [8], and with Lim and Liew [5] for the higher modes.

The final comparison concerns conical panels having free edges. Bardell et al. [8] provided two sets of experimental results, as well as theoretical results, for conical panels with completely free edges. In their

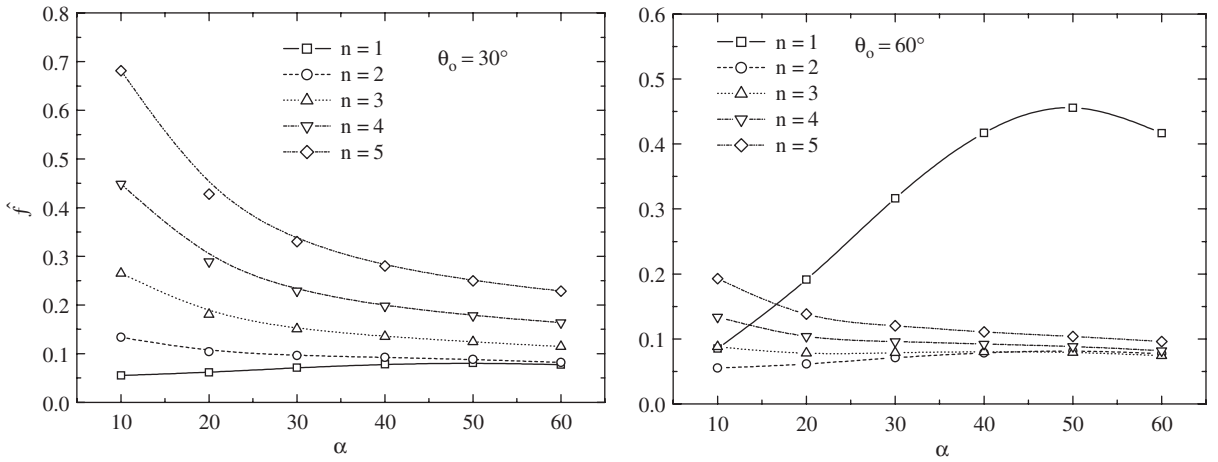

Fig. 6. Frequency parameter $\hat{f} = \omega b\sqrt{\rho h/A_{11}}$ of conical panels with F_S–F_L boundary conditions ($m = 1, v = 0.3, h/R_1 = 0.01, L/R_1 = 20$).

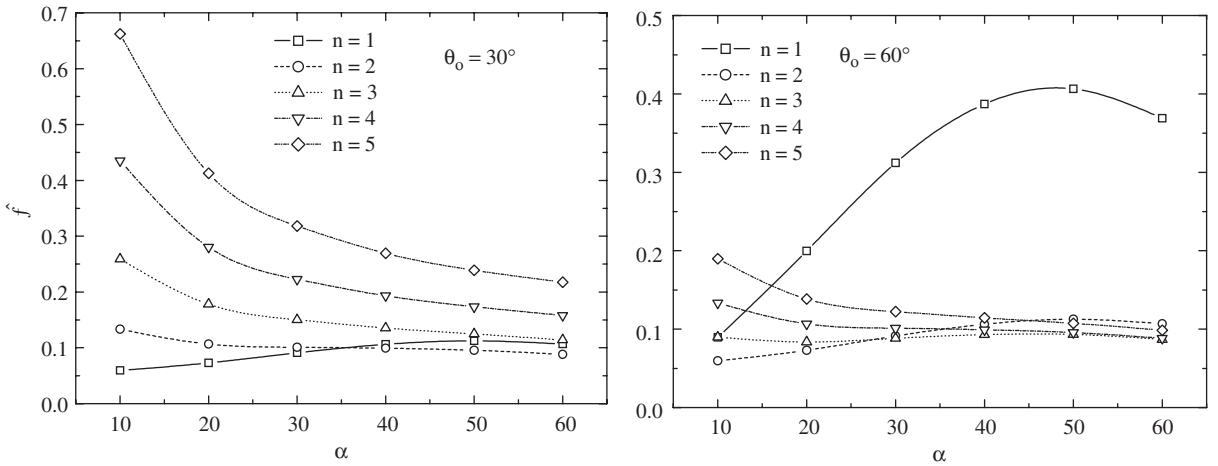

Fig. 7. Frequency parameter $\hat{f} = \omega b\sqrt{\rho h/A_{11}}$ of conical panels with F_S–C_L boundary conditions ($m = 1, v = 0.3, \theta_o = 60^\circ, h/R_1 = 0.01$, $L/R_1 = 20$).

Table 3
Comparison of frequency parameter $\tilde{f} = \omega L^2\sqrt{\rho h/D}$ for a clamped conical shell panel ($L/s = 0.6, L/h = 100, L/R_1 = 3, \alpha = 30^\circ$, $\theta_o = 60^\circ, v = 0.3$)

		$\tilde{f}_1$	$\tilde{f}_2$	$\tilde{f}_3$	$\tilde{f}_4$
Cheung et al. [4]		213.4	262.5	314.7	358.6
Bardell et al. [8]		209.84	257.11	307.9	351.90
Present 2-D *kp*-Ritz	20 × 20	214.21	278.90	329.17	380.69
	22 × 22	211.48	274.15	324.86	375.73
	24 × 24	210.72	272.26	324.25	374.13
	26 × 26	207.53	266.96	318.53	367.95

Table 4
Comparison of frequency parameter $\bar{f} = \omega L b_o \sqrt{\rho h/D}$ for conical shell panels with CFFF boundary conditions ($s/h = 1000, \alpha = 7.5^\circ, \theta_o = 30.247^\circ, \nu = 0.3$)

L/s		1	2	3	4	5	6	7	8
0.2	Lim and Liew [5]	6.1727	9.0708	27.299	29.758	50.665	65.171	74.499	80.201
	Bardell et al. [8]	5.5130	8.9563	26.989	28.852	50.174	64.497	75.479	79.578
	Present 2-D *kp*-Ritz	5.8022	9.4253	27.782	29.365	51.676	65.446	75.386	82.783
0.8	Lim and Liew [5]	3.2691	8.3659	16.521	17.117	23.907	29.891	38.614	46.687
	Bardell et al. [8]	1.6855	6.3789	15.158	16.412	23.937	28.076	38.344	45.069
	Present 2-D *kp*-Ritz	1.7094	6.4421	15.327	17.398	23.909	28.393	40.651	45.607

Table 5
The geometrical and material properties of the two completely free conical panel types

	α (deg)	L (m)	R_1 (m)	θ_o (deg)	h (m)	E (GPa)	ρ (kg/m^3)	$\bar{\nu}$
Cone 1	3.8	1.14	0.34	130	2.0	70	2700	0.3
Cone 2	26.5	1.12	0.16	180	2.0	70	2700	0.3

Table 6
Comparison of natural frequencies of a completely free conical shell panel, geometrical and material properties based on "Cone 1"

Mode	Bardell et al. [8]		Present 2-D *kp*-Ritz		
	Theoretical	Experimental	20×20	22×22	24×24
1	7.21	7.5	7.437	7.394	7.33
2	12.32	12.7	13.433	13.181	12.85
3	18.21	18.2	19.331	19.102	18.80
4	34.40	35.6	37.381	36.761	35.96
5	44.32	46.0	47.592	46.980	46.18
6	67.78	59.5	72.565	71.697	70.46
7	75.43	70.4	77.280	76.963	76.52
8	76.05	73.1	77.952	77.393	76.69
9	87.80	90.4	93.882	92.874	91.53
10	113.65	N/A	121.93	120.63	118.78

experiments, Bardell et al. [8] prepared two different aluminum conical panels for testing, which were referred as "Cone 1" and "Cone 2"; the geometric and material properties of which are summarized in Table 5. The frequencies of the first ten modes for each case are given in Tables 6 and 7. The present converged results are obtained with a support size of 3.5 and 24×24 nodes. It is observed that very good agreement is attained for both cases, especially for the lower frequencies. From these comparisons, the accuracy and stability of the present formulation are validated.

The following parametric study focuses on the effects of the semi-vertex angle α on the frequencies of the conical panels. Four sets of boundary conditions are considered in the present study, namely, (i) SSSS-simply supported at four edges, (ii) CFFF-clamped at the larger curved edge, and the other three sides free, (iii) FFFF-completely free at four sides, and (iv) CCCC-clamped at four edges. The panel parameters are $\theta_o = 60^\circ, R_1/h = 100, L/R_1 = 20$, and $\nu = 0.3$. The frequency parameter $\tilde{f}$ of the first eight modes is computed for each of the four boundary conditions, with α ranging from 15° to 75°. Fig. 8 plots the results for the SSSS

Table 7
Comparison of natural frequencies of a completely free conical shell panel, geometrical and material properties based on "Cone 2"

Mode	Bardell et al. [8]		Present 2-D *kp*-Ritz		
	Theoretical	Experimental	22 × 22	23 × 23	24 × 24
1	4.65	4.5	4.7	4.69	4.64
2	8.75	8.9	8.83	8.78	8.75
3	11.32	11.5	12.25	12.11	11.99
4	20.85	20.9	22.11	22.01	21.92
5	22.63	21.7	22.72	22.49	22.30
6	33.06	33.2	35.53	35.19	34.92
7	47.83	46.6	48.48	48.28	48.13
8	47.87	47.4	50.11	49.77	49.45
9	63.51	58.6	66.99	66.61	66.30
10	67.95	63.7	69.02	68.80	68.59

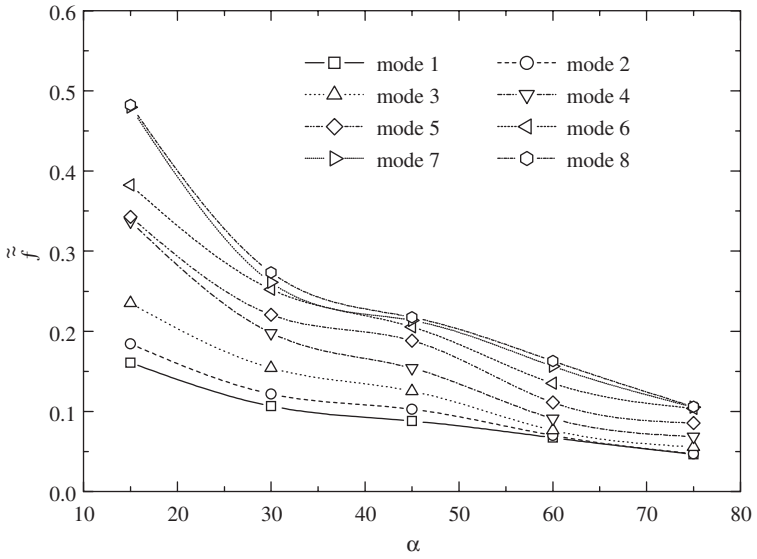

Fig. 8. Frequency parameter $\tilde{\tilde{f}} = \omega L\sqrt{\rho(1-\nu^2)/E}$ of conical panels with SSSS boundary conditions ($R_1/h = 100, L/R_1 = 20, \theta_o = 60^\circ$, $\nu = 0.3$).

case. It is observed that the frequencies of a given mode generally decrease with increasing α. This trend is also observed for most of the modes of the CFFF panels, which are presented in Fig. 9. The modes 1, 2 and 4 show slight differences from the other modes, whereby the frequency increases slightly as α varies from 15° to 30°, and then decreases as α is increased further. The frequencies of the conical panels with FFFF and CCCC boundary conditions also show similar trends as those observed for the SSSS case, and these numerical results are plotted in Figs. 10 and 11, respectively.

In this work, the feasibility of the *kp*-Ritz method for free vibration analysis to vibration studies of conical panels was demonstrated. In the conventional Ritz method, the trial functions must satisfy at least the essential boundary conditions, and it is difficult to find appropriate trial functions for certain boundary condition types. The present *kp*-Ritz method overcomes this limitation, whereby a common shape function based on the mesh-free approach is used to generally describe the interior domain. The boundary conditions are separately dealt with subsequently through penalty enforcement. The present method thus avoids the eigen

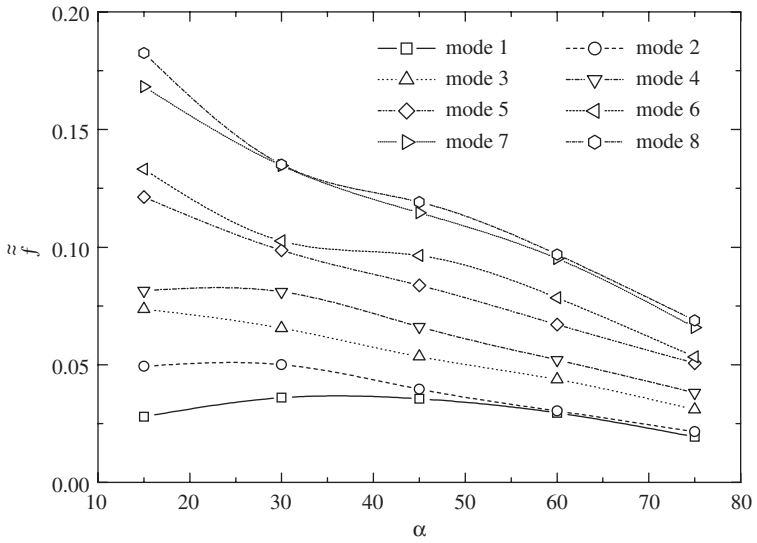

Fig. 9. Frequency parameter $\tilde{\tilde{f}} = \omega L\sqrt{\rho(1-\bar{\nu}^2)/E}$ of conical panels with CFFF boundary conditions ($R_1/h = 100, L/R_1 = 20, \theta_o = 60^\circ$, $\nu = 0.3$).

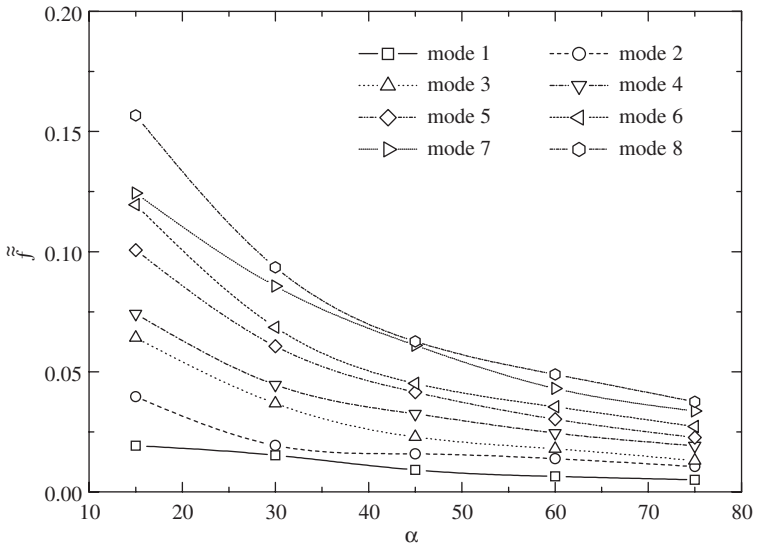

Fig. 10. Frequency parameter $\tilde{\tilde{f}} = \omega L\sqrt{\rho(1-\bar{\nu}^2)/E}$ of conical panels with FFFF boundary conditions ($R_1/h = 100, L/R_1 = 20, \theta_o = 60^\circ$, $\nu = 0.3$).

equations for each boundary case being reformulated, and the computational efforts are therefore reduced. This makes the *kp*-Ritz method more robust that the conventional Ritz method.

4. Conclusions

The free vibration analysis of conical shell panels has been carried out by the 1-D and 2-D versions of the *kp*-Ritz method. Love's hypothesis for classical thin-shells was employed in the present analyses. The 1-D *kp*-Ritz version was used for conical panels with two simply supported straight edges, where the kernel particle estimation is employed in hybridized form with harmonic functions to approximate the 2-D displacement

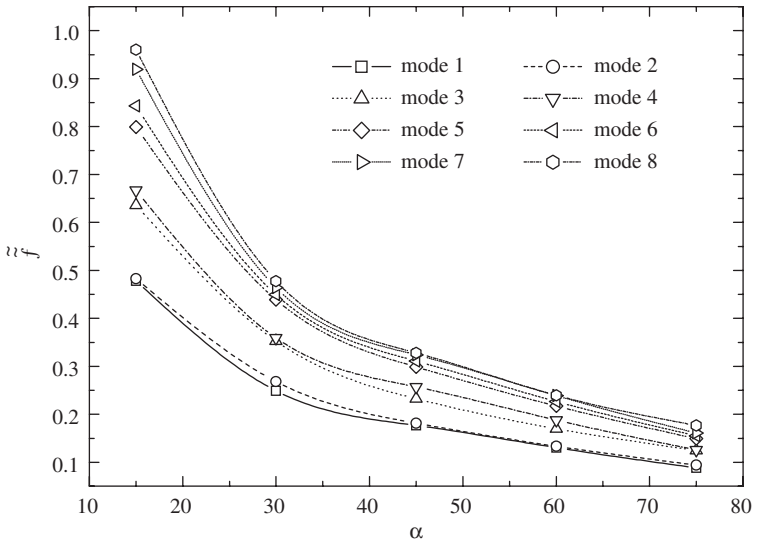

Fig. 11. Frequency parameter $\tilde{\tilde{f}} = \omega L\sqrt{\rho(1-\bar{\nu}^2)/E}$ of conical panels with CCCC boundary conditions ($R_1/h = 100, L/R_1 = 20, \theta_o = 60^\circ$, $\nu = 0.3$).

field. The 2-D *kp*-Ritz version was used for conical panels having arbitrary boundary conditions, where the displacement field is approximated by kernel particle functions in 2-D. The accuracy of the present formulations has been verified via extensive comparisons with existing results. Further, it was found that the semi-vertex angle α has no significant effects on convergence rates. From the parametric studies, it has been concluded that boundary conditions and the value of the semi-vertex angle significantly influence the frequency characteristics of the conical panels.

References

[1] J.N. Rossetos, R.F. Parisse, The dynamic response of cylindrical and conical panels, *Journal of Applied Mechanics* 36 (1969) 271–276.
[2] D. Teichmann, An approximation of the lowest eigenfrequencies and buckling loads of cylindrical and conical shell panels under initial stress, *American Institute of Aeronautics and Astronautics Journal* 23 (1985) 1634–1637.
[3] R.S. Srinivasan, P.A. Krishnan, Free vibration of conical shell panels, *Journal of Sound and Vibration* 117 (1987) 153–160.
[4] Y.K. Cheung, W.Y. Li, L.G. Tham, Free vibration analysis of singly curved shell by spline finite strip method, *Journal of Sound and Vibration* 128 (1989) 411–422.
[5] C.W. Lim, K.M. Liew, Vibratory behaviour of shallow conical shells by a global Ritz formulation, *Engineering Structures* 17 (1995) 63–70.
[6] K.M. Liew, M.K. Lim, C.W. Lim, Effects of initial twist and thickness variation on the vibration behaviour of shallow conical shells, *Journal of Sound and Vibration* 180 (1995) 271–296.
[7] C.W. Lim, K.M. Liew, Vibration of shallow conical shells with shear flexibility: a first-order theory, *International Journal of Solids and Structures* 33 (1996) 451–468.
[8] N.S. Bardell, J.M. Dunsdon, R.S. Langley, Free vibration of thin, isotropic, open, conical panels, *Journal of Sound and Vibration* 217 (1998) 297–320.
[9] K.M. Liew, Z.C. Feng, Vibration characteristics of conical shell panels with three-dimensional flexibility, *Journal of Applied Mechanics* 67 (2000) 314–320.
[10] K.Y. Lam, H. Li, T.Y. Ng, C.F. Chua, Generalized differential quadrature method for the free vibration of truncated conical panels, *Journal of Sound and Vibration* 251 (2002) 329–348.
[11] J.W. Rayleigh, *Theory of Sound*, Vol. 1, Macmillan, 1877 (reprinted by Dover Publications in 1945).
[12] W. Ritz, Uber eine neue Methode zur Losung gewisser variationsprobleme der mathematischen Physik, *Journal fur Reine und Angewandte Mathematik* 135 (1909) 1–61.
[13] K.M. Liew, K.Y. Lam, Application of two-dimensional orthogonal plate function to flexural vibration of skew plates, *Journal of Sound and Vibration* 139 (1990) 241–252.
[14] K.M. Liew, K.Y. Lam, A Rayleigh–Ritz approach to transverse vibration of isotropic and anisotropic trapezoidal plates using orthogonal plate functions, *International Journal of Solids and Structures* 27 (1991) 189–203.

[15] K.M. Liew, K.Y. Lam, A set of orthogonal plate functions for vibration analysis of regular polygonal plates, *Transactions of the ASME Journal of Vibration and Acoustics* 113 (1991) 182–186.
[16] K.M. Liew, K.Y. Lam, Vibration analysis of multi-span plates having orthogonal straight edges, *Journal of Sound and Vibration* 147 (1991) 255–264.
[17] K.M. Liew, K.Y. Lam, Vibration of skew plates by Rayleigh–Ritz method, *Journal of Sound and Vibration* 153 (1992) 535–536.
[18] K.M. Liew, Vibration of symmetrically laminated cantilever trapezoidal composite plates, *International Journal of Mechanical Sciences* 34 (1992) 299–308.
[19] K.M. Liew, Frequency solutions for circular plates with internal supports and discontinuous boundaries, *International Journal of Mechanical Sciences* 34 (1992) 511–520.
[20] K.M. Liew, A hybrid energy approach for vibrational modelling of laminated trapezoidal plates with point supports, *International Journal of Solids and Structures* 29 (1992) 3087–3097.
[21] K.M. Liew, Vibration of eccentric ring and line supported circular plates carrying concentrated masses, *Journal of Sound and Vibration* 156 (1992) 99–107.
[22] K.M. Liew, Treatments of over-restrained boundaries for doubly connected plates of arbitrary shape in vibration analysis, *International Journal of Solids and Structures* 30 (1993) 337–347.
[23] K.M. Liew, On the use of pb-2 Rayleigh–Ritz method for free-flexural vibration of triangular plates with curved internal supports, *Journal of Sound and Vibration* 165 (1993) 329–340.
[24] K.M. Liew, C.M. Wang, pb-2 Rayleigh–Ritz method for general plate analysis, *Engineering Structures* 15 (1993) 55–60.
[25] K.M. Liew, C.W. Lim, A Ritz vibration analysis of doubly curved rectangular shallow shells using a refined first-order theory, *Computer Methods in Applied Mechanics and Engineering* 127 (1995) 145–162.
[26] K.M. Liew, Y.K. Sum, Vibration of plates having orthogonal straight edges with clamped boundaries, *Journal of Engineering Mechanics ASCE* 124 (1998) 184–192.
[27] K.M. Liew, B. Yang, Elasticity solutions for free vibrations of annular plates from three-dimensional analysis, *International Journal of Solids and Structures* 37 (2000) 7689–7702.
[28] K.M. Liew, Z.C. Feng, Three-dimensional free vibration analysis of perforated super elliptical plates via the p-Ritz method, *International Journal of Mechanical Sciences* 43 (2001) 2613–2630.
[29] K.M. Liew, K.Y. Lam, S.T. Chow, Free vibration analysis of rectangular plates using orthogonal plate function, *Computers and Structures* 34 (1990) 79–85.
[30] K.M. Liew, L.A. Bergman, T.Y. Ng, K.Y. Lam, Three-dimensional vibration of cylindrical shell panels-solutions by continuum and discrete approaches, *Computational Mechanics* 26 (2000) 208–221.
[31] K.M. Liew, Y. Xiang, C.M. Wang, S. Kitipornchai, Flexural vibration of shear deformable circular and annular plates on ring supports, *Computer Methods in Applied Mechanics and Engineering* 110 (1993) 301–315.
[32] K.M. Liew, Y. Xiang, S. Kitipornchai, J.L. Meek, Formulation of Mindlin–Engesser model for stiffened plate vibration, *Computer Methods in Applied Mechanics and Engineering* 120 (1995) 339–353.
[33] C.W. Lim, K.M. Liew, A pb-2 Ritz formulation for flexural vibration of shallow cylindrical shells of rectangular platform, *Journal of Sound and Vibration* 173 (1994) 343–375.
[34] S. Kitipornchai, Y. Xiang, C.M. Wang, K.M. Liew, Buckling of thick skew plates, *International Journal for Numerical Methods in Engineering* 36 (1993) 1299–1310.
[35] Y.K. Cheung, D. Zhou, Vibrations of rectangular plates with elastic intermediate line-supports and edge constraints, *Thin-Walled Structures* 37 (2000) 305–331.
[36] Y.K. Cheung, D. Zhou, Three-dimensional vibration analysis of cantilevered and completely free isosceles triangular plates, *International Journal of Solids and Structures* 39 (2002) 673–687.
[37] Y.K. Cheung, D. Zhou, Free vibrations of rectangular unsymmetrically laminated composite plates with internal line supports, *Computers and Structures* 79 (2001) 1923–1932.
[38] J.S. Chen, C. Pan, C.T. Wu, W.K. Liu, Reproducing kernel particle methods for large deformation analysis of non-linear structures, *Computer Methods in Applied Mechanics and Engineering* 139 (1996) 195–227.
[39] W.K. Liu, S. Jun, Y.F. Zhang, Reproducing kernel particle methods, *International Journal for Numerical Methods in Fluids* 20 (1995) 1081–1106.
[40] J.N. Reddy, *An Introduction to the Finite Element Method*, McGraw-Hill, New York, 1993.
[41] J.N. Reddy, *Applied Functional Analysis and Variational Methods in Engineering*, McGraw-Hill, New York, 1986 (Reprinted by Krieger, Melbourne, FL, 1991).